Inorganic Chemistry

pubs.acs.org/IC Article

Ligand Lability Driven by Metal-to-Borane Pseudorotation: A Mechanism for Ligand Exchange

Jonathan Bould,* Oleg Tok, Vincenzo Passarelli, Michael G. S. Londesborough, and Ramón Macías*

Cite This: https://dx.doi.org/10.1021/acs.inorgchem.0c02205 Read Online

ACCESS | Metrics & More | Article Recommendations | Supporting Information

ABSTRACT: The discovery of systems that interact with small molecules plays a vital facilitating role in the development of devices that show sensitivity to their surroundings and an ability to quickly relay chemical and physical information. Herein, we report on the reaction of [$NiCl_2$(dppe)] with decaborane that produces in usable yield a new 11-vertex nickelaborane, [7,7-(dppe)-*nido*-7-$NiB_{10}H_{12}$] (**1**), which shows interesting reactivity and functionality toward carbon monoxide and ethylisonitrile. This contribution describes the synthesis and full structural characterization of **1** and its small-molecule EtNC and CO adducts, **2** and **3**, and delineates the dynamic molecular behavior of all of these species in solution. This information sets a foundation from which more advanced work on this and related metallaborane systems can be conceived and provides a more general reference to how NMR spectroscopy, combined with DFT calculations, can be used to analyze the precise locomotion of labile ligands around a metal center held within a borane cluster.

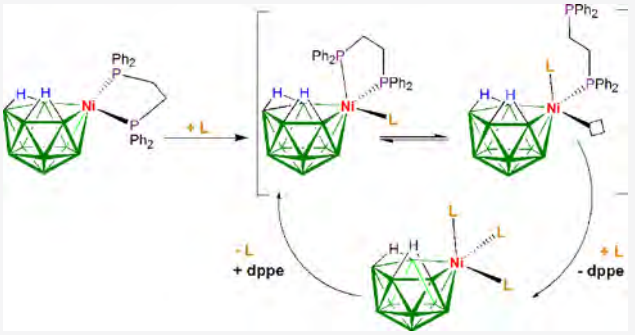

INTRODUCTION

The boron hydrides (commonly referred to as the boranes) form deltahedral cages and clusters with molecular geometries that represent an architectural "bridge" in the structural continuum that stretches from the highly condensed atomic assemblies adopted by the late transitional metals to the open chains and ring formations found in the hydrocarbons. Into the framework of these deltahedral boranes can be incorporated elements from throughout the periodic table, giving rise to a whole series of molecular compounds often referred to as heteroboranes, in which the heteroatoms fit into the polyhedral architectural principles of the borane clusters.[1] In the case of metal centers, the resulting metallaboranes[2,3] and metalla-heteroboranes feature borane/heteroborane fragments that can be regarded as polyhapto face-bound ligands to the incorporated metals. Metallaboranes and metallaheteroboranes are thus polyhedral molecules of hybrid borane cluster-metal structural character that is quite different from that of the better-understood organometallic complexes. As structure is often the determinant of chemical properties, the unusual molecular structures of metallaborane and metallaheteroborane clusters promise novel chemical functionality. One example of this principle, relevant to this contribution, is the activation of small molecules on metallaborane compounds and their further modification in catalytic cycles. The rhodathiaboranes, [8,8-$(PPh_3)_2$-*nido*-8,7-$RhSB_9H_{10}$] and [2,2,2-(H)$(PPh_3)_2$-*closo*-1,2-$RhSB_8H_8$] have been shown to be catalytically active.[4,5] In another system, the icosahedral bimetallaborane compounds of type [$L_4M_2B_{10}H_{10}$] (where L is typically a phosphine and M is either Pd or Pt) will reversibly take up small molecules such as O_2, CO, and SO_2 across their M−M cluster edge in a process controllable by pressure, UV irradiation, or sequestered-ligand displacement.[6,7] In both cases, the borane cluster plays a critical role in the molecular functionality. In the latter example of the bimetallic compounds, it is the boron polyhedral cage that holds the adjacent metal atoms in the appropriate geometry to facilitate the reversible uptake of small molecules. In the former example, the metallathiaborane compounds exhibit two principal points of reactivity: the metal center together with an adjacent boron B−H unit, which together enable a catalytic activity that encompasses nido to closo dehydrogenations,[8] dihydrogen-promoted closo to nido transformations,[9] oxidative additions of C−H bonds to the metal centers,[8] proton-assisted H_2 activation,[10] and the catalytic hydrogenation and isomerization of olefins.[9]

More recently, we have shown that the earth-abundant metals, nickel and iron, can also be integrated into thiaborane clusters.[11] Among the several metallathiaboranes produced in this study, the 11-vertex nickelathiaborane [8,8-$(dppe)_2$-*nido*-8,7-$NiSB_9H_{11}$] demonstrated the reversible uptake of ammonia

Received: July 24, 2020

https://dx.doi.org/10.1021/acs.inorgchem.0c02205
Inorg. Chem. XXXX, XXX, XXX−XXX

Table 1. ^{11}B and ^{1}H and Data for [(dppe)NiB$_{10}$H$_{12}$] (1), [(EtNC)(dppe)NiB$_{10}$H$_{12}$] (2), [(CO)(dppe)NiB$_{10}$H$_{12}$] (3), and [(EtNC)$_3$NiB$_{10}$H$_{12}$] (4) at 300 K in CD_2Cl_2 Solution Together with DFT-GIAO Calculated Boron Shieldings

	1			2			3			4	
assignment	δ(^{11}B)[a]	calc	δ (^{1}H)	δ (^{11}B)[a]	calc	δ (^{1}H)	δ (^{11}B)[b]	calc	δ (^{1}H)	δ(^{11}B)[b]	δ (^{1}H)[b]
5	+13.4[140]	+16.5	+3.80	+19.6[120]	+24.1	+3.34	+21.1	+27.0	+3.27	+20.0[122]	
2, 3	+17.1[125]	+21.7	+3.35	+14.5[126]	+18.5	+3.91	+16.6[113]	+20.3	+3.83	+14.3[136]	
8, 11	+11.9	+13.0	+3.17	+10.7[c]	+13.4	+2.50	+12.6	+16.0	+3.11	+10.2[117]	
1	+5.9[134]	+12.3	+2.98	−2.1[131]	+3.1	+2.54	+0.8	+5.3	+2.92	−3.2[131]	
9, 10	−1.2[d]	+3.4	+2.50	−5.3[c]	−1.0	+2.1	−3.6	+0.5	+2.49	−6.2[119]	
4, 6	−21.1[142]	−20.7	+0.87	−22.8[135]	−22.8	+0.80	−22.3[142]	−22.0	+0.90	−23.0[146]	
μH			−1.92			−2.60			−1.96		−2.14
C_2H_4			+2.36[e]			[f]			+2.54		[g]
phenyl			7.50 to 7.63			7.33 to 7.89[h]			7.31 to 7.76[h]		[g]

[a]Doublets, with ^{2}J(^{11}B−^{1}H)/Hz given in [brackets] for resonances sharp enough to be measurable. [b]Terminal hydrogen atom resonances obscured by the large excess of EtNC. [c]Shows coupling to bridging protons at −2.60 ppm; doublets broadened by unresolved coupling to bridging hydrogen atoms. [d]Shows strong coupling to bridging protons at −1.92 ppm. [e]Multiplet. [f]See Table S1. [g]Obscured by EtNC resonances. [h]Measured at −50 °C.

and carbon monoxide at the metal vertex.[11] Here, there are significant cost advantages in the use of nickel over rhodium. However, the synthesis yields of nickelathiaborane are much lower than those of the related rhodium species mentioned above. Therefore, we set upon an alternative strategy for the incorporation of nickel into decaborane, *nido*-$B_{10}H_{14}$. Decaborane is readily available and easily handled, and its deprotonated form is known to form metal complexes in a straightforward manner; the resulting *nido*-metallaundecaboranes constitute one of the best-represented metallaborane polyhedral types with the number of known compounds being about 100.[2] Thus, the reaction of [$NiCl_2$(dppe)] with decaborane afforded in usable yield and good product selectivity a new 11-vertex nickelaborane, [7,7-(dppe)-*nido*-7-$NiB_{10}H_{12}$] (**1**), which shows interesting reactivity toward carbon monoxide and ethylisonitrile, the intricacies of which are the subject of this account.

RESULTS AND DISCUSSION

Synthesis and Molecular Structure of Compound 1. Deprotonation of *nido*-decaborane with potassium triethylborohydride in diethyl ether, followed by the addition of dichloro(1,2-bis(diphenylphosphino)ethane)nickel(II), affords 11-vertex nickelaborane [7,7-(dppe)-*nido*-7-$NiB_{10}H_{12}$] (**1**) in 34% yield (eq 1):

$$\textit{nido}\text{-}B_{10}H_{14} + 2K[HBEt_3] + [Ni(Cl)_2(dppe)] \rightarrow [(dppe)\text{-}\textit{nido}\text{-}NiB_{10}H_{12}] + 2KCl + 2H_2 + 2BEt_3 \quad (1)$$

Compound **1** is characterized by NMR spectroscopy (Tables 1 and 2), elemental analysis, and single-crystal X-ray diffraction. An ORTEP drawing of the molecule is shown in Figure 1, together with selected interatomic dimensions. It may be noted that the asymmetric unit contains one molecule of chloroform solvent with a short distance of 2.05 Å between the terminal hydrogen atom on B(1) and the hydrogen atom on the chloroform solvent molecule, thus indicating a possible dihydrogen bonding interaction (i.e., <2.40 Å). These single crystals were obtained from hexane diffusion into a $CHCl_3$ solution of the compound, but initial attempts at using CH_2Cl_2 as the solvent produced poor-quality crystals with disordered solvent in the unit cell.

Table 2. ^{31}P−{^{1}H} NMR Data Measured in CD_2Cl_2 Solution at 202 MHz for [(dppe)NiB$_{10}$H$_{12}$] (1), [(EtNC)(dppe)NiB$_{10}$H$_{12}$] (2), and [(CO)(dppe)NiB$_{10}$H$_{12}$] (3)

compound	temp/K	δ(^{31}P)/ppm	relative intensity ratio[a]	coalescence temp/K
1	300	+55.3(s)		
2a		+39.2(d), +38.2(d)[b]	0.7(65)	238
2b	193	+54.4(s)[c]	0.3(35)	303
3a		+40.0(d), +39.5(d)[c]	0.2(13)	
3b	178	+57.5(s)	0.8(87)	

[a]The overall integrated relative intensities of the resonances. DFT calculated Boltzmann populations are in parentheses. [b]Doublets, ^{2}J(^{31}P−^{31} P) 33 Hz. Higher field resonance is relatively broader and is probably P(1) trans to B(8). [c]Doublets ^{2}J(^{31}P−^{31} P) 23 Hz.

Structurally, the compound is analogous to a number of *nido*-metallundecaborane clusters such as [8,8-$(PPh_3)_2$-*nido*-8,7-$RhSB_9H_{10}$],[12] [μ-2,7-(SCSNEt)(PMe_2Ph)-*nido*-$PtB_{10}H_{11}$],[13] [$(PMe_2Ph)_2$-*nido*-$MB_{10}H_{12}$] (M = Pt,[14] Pd[15]), and the nickelathiaborane analogue [8,8-(dppe)-*nido*-8,7-$NiSB_9H_{11}$].[11] The presence of the nickel vertex reduces the metal−B distances in the metallaborane cluster, for example, Ni(7) to B(8) and B(11) are 2.207(5) and 2.183(5) Å in **1** compared to 2.324(2) and 2.314(2) Å in [$(PMe_2Ph)_2$-*nido*-$PdB_{10}H_{12}$].[14] The ca. 0.12 Å shortening reflects the smaller covalent radius of Ni (1.24 Å) compared to that of Pd (1.39 Å).[16] The structure differs considerably from that of thiaborane analogue [8,8-(dppe)-*nido*-8,7-$NiSB_9H_{11}$][11] in which a B−H vertex is subrogated by a sulfur atom and the two bridging B−H−B hydrogen atoms occupy different positions on the pentagonal open face (schematic structures in Scheme 1). These structural changes can be rationalized as a consequence of different metal-to-ligand interactions, a point that is discussed in the next section.

Electron Counting and Bonding Considerations. Electron-counting rules[17−19] require that the structure of 11-vertex *nido*-nickelaborane (**1**), based on a 12-vertex icosahedron with 1 vertex missing, needs 13 skeletal electron bonding pairs (SEP). By these conventions, the addition of the {dppeNi}$^{2+}$ moiety and no skeletal electrons to the 10-vertex 12-SEP $[B_{10}H_{12}]^{2-}$ should result in a closo structure. That the

https://dx.doi.org/10.1021/acs.inorgchem.0c02205
Inorg. Chem. XXXX, XXX, XXX−XXX

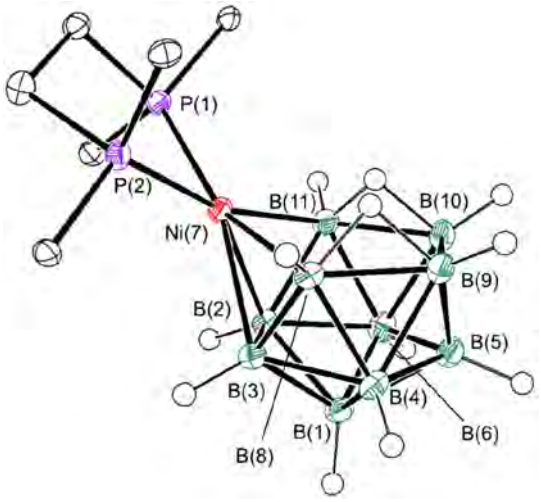

Figure 1. Drawing of the molecular structure of [7,7-(dppe)-*nido*-7-$NiB_{10}H_{12}$]·$CHCl_3$ (**1**) with 50% probability ellipsoids for heavy atoms. To aid clarity, the solvent molecule is not shown. Selected distances (angstroms): from Ni(7) to B(2), 2.117(3); to B(3), 2.115(3); to B(8), 2.203(3); to B(11), 2.211(3); to P(1), 2.2109(7); and to P(2), 2.1943(7). Distance (angstroms) from B(9) to B(10), 1.990(5). Angles (deg): P(1)−Ni(7)−P(2), 85.91(8); P(1)−Ni(7)−B(11), 85.91(8); P(1)−Ni(7)−B(8), 158.18(9); P(2)−Ni(7)−B(11), 88.36(14); and P(2)−Ni(7)−B(8), 94.74(14).

Scheme 1. Comparison between 11-Vertex *nido*-Nickelaborane (1) and Its *arachno*-Nickelathiaborane Counterpart, Tracing the Changes upon Metalation and BH Unit Subrogation by Sulfur

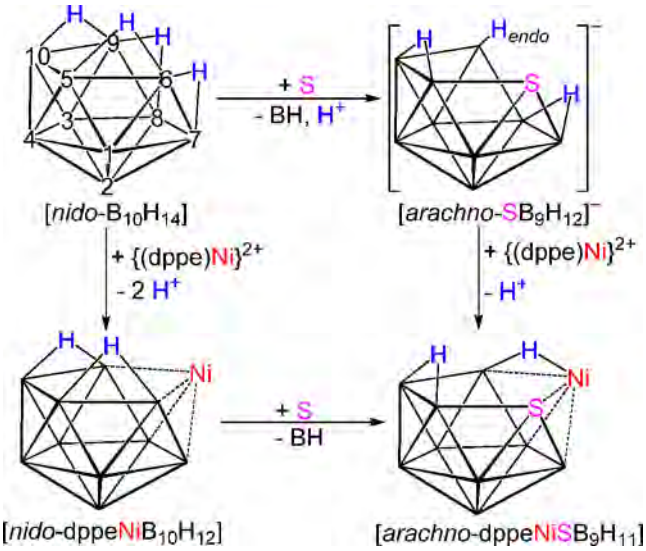

observed molecule has nido structure is, however, not surprising: it is well documented that metallaboranes and metallathiaboranes featuring pseudo-square-planar metal centers in the cluster framework often deviate from the dictates of the electron-counting rules.[20−22] Specifically, in the case of these metallaundecaborane clusters, one electron pair, which is included in the skeletal electron count, is localized on the two bridging hydrogen atoms on the open pentagonal face. These B−H−B hydrogen atoms sterically "block" the attainment of a closo structure. Thus, in the case of the nido 11-vertex rhodathiaundecaborane compound $[(PPh_3)_2RhSB_9H_{10}]$, it is experimentally observed that the deprotonation of the cluster-bridging hydrogen atom affords the closo anion, $[(PPh_3)_2$-*closo*-$RhSB_9H_9]^-$, although there is no change in the skeletal-electron count. The structural change is reversed on reprotonation.[21,23]

These considerations suggest that the {dppeNi} group interacts with the $\{B_{10}H_{12}\}$ fragment by forming two main bonding vectors directed toward the B2−B11 and B3−B8 edges, formally subrogating two μ-H hydrogen atoms on the decaborane cluster. The two Ni−P *exo*-polyhedral bonds complete the coordination sphere around the metal center. Therefore, compound **1** could be tentatively described as a pseudo-square-planar Ni(II) complex in which the $[B_{10}H_{12}]^{2-}$ fragment acts as a tetrahapto dianionic ligand (schematic structure **I**, Scheme 2). This description would imply a two-orbital contribution of the nickel fragment to cluster bonding.

Scheme 2. Metal-to-Borane/Thiaborane Bonding Vectors and Suggested Coordination Modes for [7,7-(dppe)-*nido*-7,7-$NiB_{10}H_{12}$] and [8,8-(dppe)-*nido*-8,7-$NiSB_9H_{11}$]

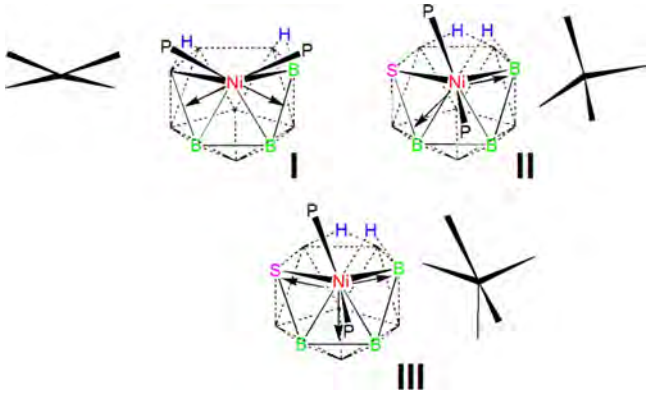

In [8,8-(dppe)-*nido*-8,7-$NiSB_9H_{11}$], with two bonding vectors directed toward the B9 vertex and toward the face-bonded S7−B3−B4 region of the thiaborane ligand, it would imply a pseudo-tetrahedral coordination mode around the nickel(II) center, with the $[SB_9H_{11}]^{2-}$ anion acting as a tetrahapto bidentate ligand (Scheme 2, **II**). Alternatively, we could describe three main nickel-to-thiaborane interactions with bonding vectors directed toward the B9 vertex, the B3−B4 edge, and the sulfur atom, which, together with the two Ni−P bonds, forms a pentacoordinated Ni(II) complex. The $[SB_9H_{11}]^{2-}$ anion could be regarded, therefore, as a tetrahapto ligand that features tridentate coordination (Scheme 3, **III**).

This qualitative bonding analysis reveals that although the nickelaborane and the nickelathiaborane can both be described as 11-vertex nido clusters, the nickel-to-borane/thiaborane interaction differs, and this difference is reflected in the molecular structure of the clusters. For example, the dihedral angle Φ between the P1−Ni7−P2 and the B8−Ni7−B11 planes in **1** is 4.71°, whereas for the equivalent P1−Ni−P2 and the B−Ni−S planes in $[(dppe)NiSB_9H_{11}]$ it is 96.1°. In fact, a variation in the orientation of the $\{L_2M\}$ moiety with respect to the $\{\eta^4$-$B_{10}H_{12}\}$ cluster, as delineated by the L−M−L/B(8)−M−B(11) dihedral angle (numbered as in **1**), is a feature in this class of compounds. In $[(PMe_2Ph)_2MB_{10}H_{12}]$, it is ca. 21 and 11° for Pt and Pd, respectively.[15] This structural feature is also found in 11-vertex metallathiaboranes that incorporate $\{L_2M\}$ fragments, where M = Rh, Ir, or Pt. Thus, in the dppe-ligated rhodathiaborane, [8,8-(dppe)-8,7-$RhSB_9H_{10}$], the angle is 69°, a value that is closer to that

https://dx.doi.org/10.1021/acs.inorgchem.0c02205
Inorg. Chem. XXXX, XXX, XXX−XXX

Scheme 3. Reactions of [7,7-(dppe)-*nido*-7-$NiB_{10}H_{12}$] (1) with EtNC and CO to Give Adducts [(EtNC)(dppe)-*nido*-$NiB_{10}H_{12}$] (2) and [(CO)(dppe)-*nido*-$NiB_{10}H_{12}$] (3)[a]

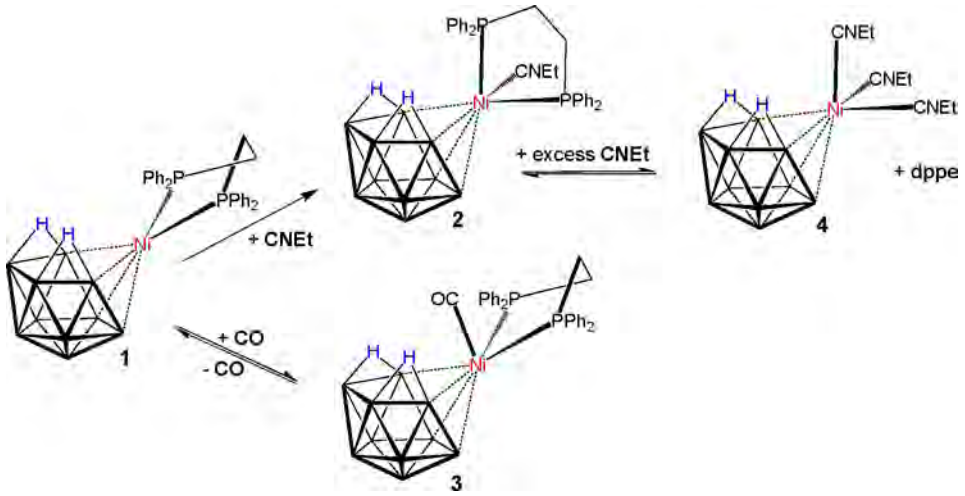

[a]The addition of a large excess of EtNC to **2** affords [$(EtNC)_3$-*nido*-$NiB_{10}H_{12}$] (**4**).

found for the dppe-ligated nickelathiaborane than to that found for **1**.

Although these variations are significant in the solid state, we should note that in solution the metal-to-borane/thiaborane interaction is often labile, leading to mutual contra-rotation of the metal group with respect the borane/thiaborane fragment, a fluxional process that is often observable in solution on the NMR time scale.[15] The variation in the dihedral angle, therefore, may also be seen as a consequence of packing forces in the crystal structure.

Compound **1** was also characterized by NMR spectroscopy (Tables 1 and 2, Figures S1 and S2). The room-temperature $^{11}B-\{^1H\}$ NMR spectrum exhibits six resonances with a 2:1:2:1:2:2 relative intensity ratio between +17.1 and −21.1 ppm. The ^1H NMR spectrum shows six resonances between +3.80 and +0.87 ppm that correspond to the B−H terminal hydrogen atoms, and these were assigned to their directly bound boron atoms by ^1H NMR with selective $^1H-\{^{11}B\}$ experiments. This procedure, together with DFT-GIAO calculations,[24] allows us to assign the boron and proton resonances to their positions in the cluster, and these assignments match those in the literature for the platinum analogue, $[(PMe_2Ph)_2PtB_{10}H_{12}]$.[25] The $^1H-\{^{11}B\}$ NMR spectrum shows a single resonance for the two B−H−B bridging hydrogen atoms at δ(H), −1.92 ppm. In the case of compound **1**, we did not observe the sort of fluxional contra-rotation found in related platina and palladaphosphino analogoues, [$(PMe_2Ph)_2$-*nido*-$MB_{10}H_{12}$] (M = Pt, Pd), mentioned above.[14,15]

Reactions of 1 with CO and EtNC. Treatment of **1** with Lewis bases C≡N−Et and C≡O affords the corresponding nickel adducts, [7,7,7-(L)(dppe)-*nido*-7-$NiB_{10}H_{12}$], where L = CN−Et (**2**) and CO (**3**) (Scheme 3).

The attachment of carbon monoxide to the {Ni(dppe)} center is weak and easily reversible, with the evacuation of the CO atmosphere leading to CO loss and the regeneration of **1**, indicating that there is an equilibrium between the parent nickelaborane, **1**, and the CO adduct, **3**, as illustrated in Scheme 3. Thus, a large excess of carbon monoxide is needed for the reaction to proceed. Because of the lability of the carbonyl bond, the CO-ligated compound, **3**, was characterized solely by NMR spectroscopy. From NMR measurements, it is clear that the sequestration of CO by **1** is immediate. However, over a period of 2 days at 20 °C a sample of **3** sealed in a Teflon-capped NMR tube under a CO atmosphere completely decomposes to afford decaborane (*nido*-$B_{10}H_{14}$) as the only polyhedral boron-containing compound present. The production of decaborane demonstrates that the {dppeNi} moiety undergoes elimination from the 11-vertex nickelaborane cage. This process is unclear, but we can hypothesize that the decomposition should involve the formation of nickel carbonyl species and the concomitant reduction of the $\{B_{10}H_{12}\}$ fragment to give decaborane. In comparison, the ethylisonitrile ligand forms the stable [7,7,7-(EtNC)(dppe)-*nido*-$NiB_{10}H_{12}$] (**2**) adduct in dichloromethane solution that may be isolated by thin-layer chromatography (TLC) in air. Alternatively, in concentrated $CHCl_3$ solution, the product precipitates upon addition of the isonitrile, leading to its convenient separation by simple filtration.

*Spectroscopic and Structural Characterization of **2** and **3**.* The isonitrile and carbonyl ligated compounds, **2** and **3**, respectively, are characterized by multielement NMR spectroscopy (Tables 1, 2, and S3, Figures S3−S5), together with a single-crystal X-ray diffraction analysis for **2**. Figure 2 is an ORTEP drawing of the molecule, together with selected interatomic dimensions. The molecular structure maintains the main features found in parent cluster **1**, such as the 11-vertex nido cage that can be formally derived from an icosahedron by the removal of a vertex and the presence of two B−H−B bridging hydrogen atoms along the B(8)−B(9) and B(10)−B(11) edges of the pentagonal {Ni(7)B(8)B(9)B(10)B(11)} face. The isonitrile ligand binds to the nickel center in the equatorial plane of the cluster, trans to the B(11) vertex.

Structurally, the effect of the introduction of the isonitrile ligand is to alter the orientation of the {dppeNi} moiety with respect to the pentagonal {Ni(7)B(8)B(9)B(10)B(11)} face of the cluster, rotating it by about 90° compared to that in **1**. The {dppeNi} center may be viewed as going from a 16-electron square-planar coordination to a pseudo-octahedral 18-electron center. The Ni(7)−B(8) vector, which remains trans to a dppe ligand phosphorus atom in both compounds, is unchanged in distance within experimental error [2.207(5), **2**;

https://dx.doi.org/10.1021/acs.inorgchem.0c02205
Inorg. Chem. XXXX, XXX, XXX−XXX

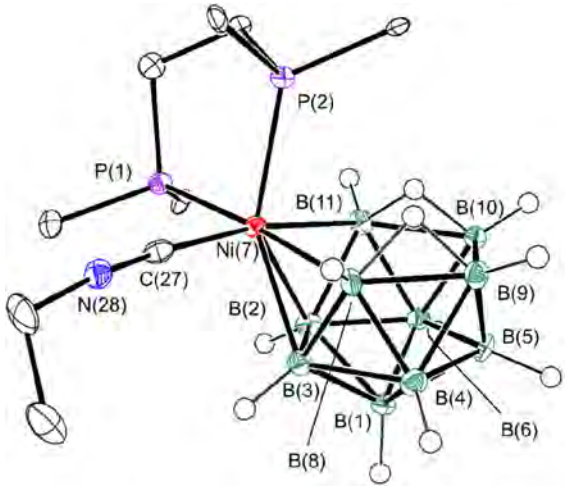

Figure 2. Drawing of the molecular structure of [(dppe)(EtNC)-*nido*-$NiB_{10}H_{12}$] (**2**) with 50% probability ellipsoids for non-hydrogen atoms. Phenyl rings, except for the ipso carbon atoms, are not shown in order to aid clarity. Selected interatomic distances (angstroms) for **1**: Ni(7) to P(1), 2.2704(12); to P(2), 2.2740(12); to C(27), 1.871(4); to B(2), 2.136(5); to B(3), 2.137(5); to B(8), 2.207(5) and to B(11), 2.183(5). Interatomic distances (angstroms): C(27)−N(28), 1.145(5) and B(9)−B(10), 1.918(7). Angles (deg): P(1)−Ni(7)−P(2), 88.39; C(27)−Ni(7)−P(1), 91.25(13); C(27)−Ni(7)−P(2), 100.18; N(28)−C(27)−Ni(7), 175.1(4).

2.203(3), Å **1**], whereas the Ni(7)−B(11) distance, in which the boron vertex is now trans to the isonitrile ligand, is slightly lengthened by ca. 0.028(6) Å.

Variable-temperature NMR measurements (discussed in detail later) show the presence of a fluxional process in both compounds **2** and **3** that involves two conformational isomers **2a**, **2b** and **3a**, **3b**. The more stable compound **2** was better suited to detailed NMR characterization, and thus the dppe and EtNC ligand region can be well characterized for the two conformers by HMBC ($^1H-^{31}P$), HSQC ($^1H-^{13}C$), and proton COSY techniques (Figure S5, Table S1).

The room-temperature $^{11}B-\{^1H\}$ NMR spectra of **2** and **3** are quite similar and exhibit six resonances in a 1:2:2:1:2:2 relative intensity ratio, between ca. +21 and −23 ppm, which is a slighter wider interval than that found for **1**. The ^1H NMR spectra show also six resonances between +3.91 and +0.80 ppm that correspond to the B−H terminal hydrogen atoms. The assignment of the proton resonances to their directly bound boron atoms was also made on the basis of ^1H NMR experiments with ^{11}B-selective decoupling together with DFT calculations of chemical shieldings. The proton resonances corresponding to the B−H−B bridging hydrogen atoms on the open pentagonal cluster face are at $\delta(H)$ −2.60 and −1.96 ppm for **2** and **3**. These proton chemical shifts, compared with the values found for **1**, imply a shift toward low frequency of 0.68 ppm for the isonitrile derivative, whereas for the CO-ligated counterpart the shift is significantly smaller at 0.04 ppm (Table 1). The presence of different ligands on the metal produces very little change in the ^{31}P chemical shifts of the phosphorus resonances between **2** and **3** (Table 2).

A comparison of the ^{11}B NMR spectra between the nickelaboranes and decaborane, depicted in Figure 3, reveals that the attachment of the Lewis bases at the nickel center does not result in a significant change in the ^{11}B NMR pattern. Compared to the parent decaborane cage, the ^{11}B NMR spectra of the nickelaboranes show an overall deshielding. The largest changes correspond to the ^{11}B resonances of the B(2,4) and B(5,7,8,10) vertices. The former resonance undergoes a ca. 20 ppm shift toward high frequency, whereas the latter ^{11}B NMR signal (of relative intensity 4) splits into two peaks that correspond to the B(2,3) and B(9,10) vertices. The resonance of the B(2,3) vertices is also shifted by ca. 20 ppm toward high frequency with respect to the equivalent signal, B(5,7,8,10), in decaborane. It should also be noted that the ^{11}B chemical shift corresponding to the B(1) vertex, opposite to the Ni(7) fragment, undergoes a significant low-frequency shift upon metalation of the boron fragment and addition of the Lewis bases, CO and CNEt, at the metal center.

From this comparison, we can see that the formal subrogation of the B−H−B bridging hydrogen atoms in the decaborane by the {dppeNi} moiety in **1** especially affects the boron vertices that lie trans to the metal and to those that bind to it directly.

Stereochemical Nonrigidity. The $^{31}P-\{^1H\}$ spectrum of parent cluster **1** shows a singlet at +55.3 ppm at 300 K, which remains the same down to 193 K, indicating that the two phosphorus nuclei are equivalent on the NMR time scale. This observation agrees with the molecular structure shown in Figure 1 and discussed above since the cluster exhibits a pseudo-plane of symmetry bisecting the cage. However, EtNC and CO adducts **2** and **3**, respectively, exhibit ^{31}P NMR spectra that change with temperature, showing the presence of two different exchange processes. Thus, for **2**, the $^{31}P-\{^1H\}$ spectrum at 273 K contains two very broad resonances at +53

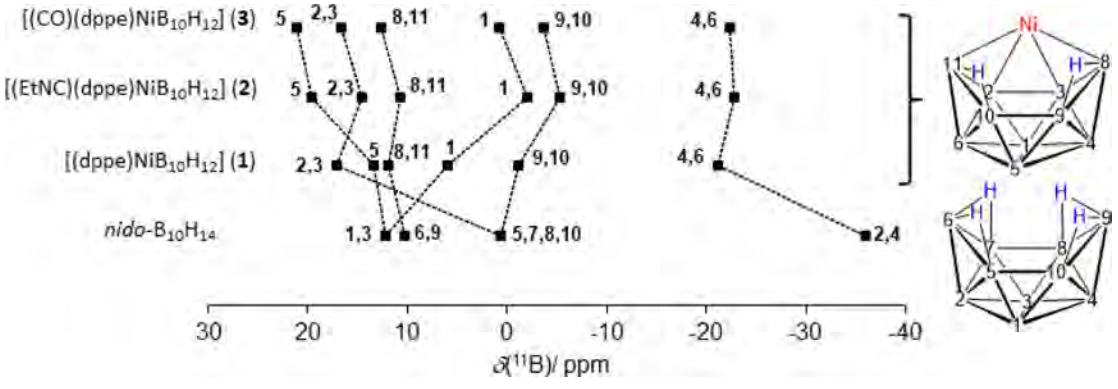

Figure 3. Representation of the chemical shifts and relative intensities in the ^{11}B NMR spectra of **3**, **2**, **1**, and *nido*-$B_{10}H_{14}$. Hatched lines connect equivalent sites. The numbering convention for 10-vertex and 11-vertex nido-type clusters is indicated on the right side of the drawing.

https://dx.doi.org/10.1021/acs.inorgchem.0c02205
Inorg. Chem. XXXX, XXX, XXX−XXX

ppm (integral intensity 0.61) and +38 ppm (integral intensity 1.00) which coalesce at ca. 300 K. On cooling to 233 K, the high-field resonance splits into two broad peaks, which become two sharp doublets with $^2J(^{31}P,^{31}P)$ = 33 Hz at 193 K, whereas the low-field signal remains a singlet at this temperature (Figure 4). Hence, there are two distinct dynamic processes

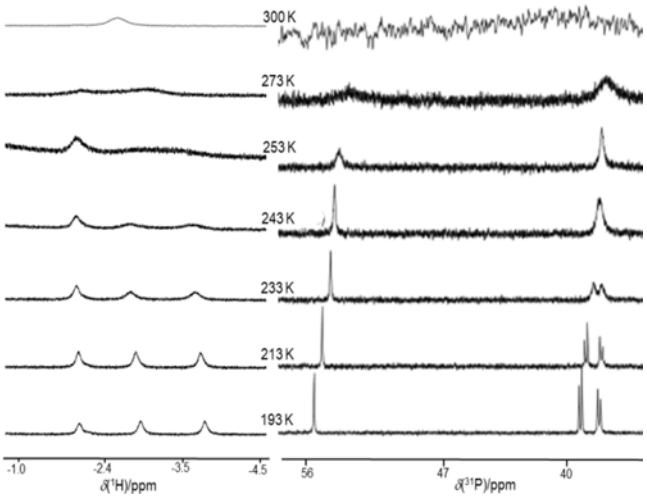

Figure 4. NMR spectra [400 MHz $^1H-\{^{11}B\}$ (left) and 202 MHz $^{31}P-\{^1H\}$ (right)] of [7,7,7-(CNEt)(dppe)-*nido*-7-$NiB_{10}H_{12}$] (**2**) in CD_2Cl_2 solution at different temperatures. The proton spectra show only the resonances corresponding to the B−H−B bridging hydrogen atoms.

involved. We assume that the high-field AB system belongs to unsymmetrical **2a** (schematic structure **I**), which is exchanging with lower-field symmetrical **2b** (schematic structure **II**), in which there are two equivalent phosphorus atoms in equatorial positions and an EtNC ligand in an axial position. We interpret the higher-energy process as arising from this 180° rotation of the ligand sphere with respect to the borane cage exchanging the two phosphine sites.

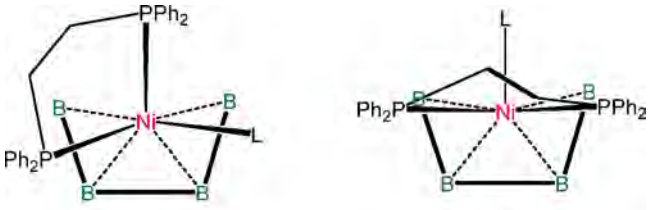

I L = EtNC **2a**, CO **3a** **II** L = EtNC **2b**, CO **3b**

This type of behavior is similar to that observed in many metallaundecaborane clusters and was first described for $[(PMe_2Ph)_2PtB_{10}H_{12}]$,[14] where it was rationalized as a mutual contra-rotation of the $\{\eta^4\text{-}B_{10}H_{12}\}$ and $(PMePh)_2$ ligands about the Pt atom with a measured activation energy of $\Delta G^{\ddagger}$ = 19 kcal mol^{-1} ($\Delta G^{\ddagger}$ = 16 kcal mol^{-1} for the Pd analogue).[14,15] Related processes have also long been known to occur in organometallic metal carbonyl complexes, where it is common to find fluxional systems that involve the pseudorotation of a $M(CO)_n$ fragment around a polyhapto carbon-bound π-ligand.[26]

For **3**, the relative intensities of the singlet and doublet ^{31}P resonances are ca. 0.2(**3a**) to 0.8(**3b**) (Figure S6). Therefore, the CO-ligated system exhibits an opposite behavior compared to that of **2**, with the symmetric conformer being the major isomer in solution at all temperatures. The variable-temperature $^1H-\{^{11}B\}$ resonances of the cage bridging hydrogen atoms for both compounds also feature similar behavior (Figure S7).

DFT calculation of the energies of the rotamer species, in which the phenyl groups are replaced by H in order to reduce the computational load, affords Boltzmann populations for the two rotamers of both **2** and **3** that agree with the NMR data (Table 2). In addition, the calculations show that, for **2**, asymmetric species **2a** is lower in energy than **2b**, whereas for **3**, the symmetrical conformer is the lowest in energy and the calculated energy difference in the species afford Boltzmann populations (62:38 calcd vs 70:30 meas for **2** and 12:88 calcd vs 22:78 meas at 193 K) that roughly reproduce the relative intensity ratios of the phosphorus resonances for both compounds. At the level of calculation employed for and the use of models in which the phenyl and other groups are replaced by hydryls and the ethyl is replaced by methyl in order to reduce the computational load demands, we should interpret this particular good correlation between experimental and calculated data with caution.

The thermodynamic parameters for the higher-energy pseudorotation of **2** for unequally populated sites were calculated via the Shanan−Atidi−Bar−Eli procedure (SI, p 18)[27] and give values of $\Delta G_{303}^{\ddagger}$ = 12.9 kcal mol^{-1} for conformer **I** → **II** and 12.4 kcal mol^{-1} for **II** → **I**, measured in the VT $^{31}P-\{^1H\}$ spectra. The coalescence temperatures of the bridging proton resonances gave Gibbs free energy barrier values of $\Delta G_{273}^{\ddagger}$ = 12.4 and 11.9 kcal mol^{-1} for **II** → **I** and **I** → **II**, respectively.

We note that the chemical shift of the low-field singlet at +54.4 ppm in this dynamic process is very similar to that in **1** (+55.3 ppm), suggesting that the dynamic process might, alternatively, involve a dissociation of the EtNC ligand to give **1** + EtNC. However, the relative intensity ratios of the resonances in **2** remain unaffected both in a CD_3CN solution and with a 10-fold equivalent excess of EtNC in CD_2Cl_2 solution. The boron spectrum at −30 °C shows the pair of resonances at $\delta(^{11}B)$ −2 to −5 ppm in **2** beginning to separate due to the presence of the two rotamer species (Figure S8) but clearly with no boron resonance at +5.9 ppm attributable to compound **1**. Additionally, the clean, tight movement up the TLC plate mentioned earlier would also tend to suggest against it. Together, these factors reasonably discount the presence of a mechanism involving a dissociative equilibrium.

Low-temperature 2D $[^{31}P-^{31}P]$-EXSY NMR spectra[28,29] clearly show the presence of two different dynamic processes, as, with the chosen exchange time and temperature of 218 K and 0.02 ms, the spectrum shows cross-peaks between the two high-field doublets for **2b** in the 1D $^{31}P-\{^1H\}$ spectrum (Figure S9). The absence of equal intensity cross peaks with singlet species **2a** under these conditions indicates that **2a** is not exchanging with **2b**. However, the EXSY spectrum at 223 K and a 0.2 s mixing time (Figure S9) exhibits cross peaks confirming that **2a** and **2b** undergo exchange. The activation parameters of the fast process (the broadness of the lines in the slower, higher-temperature exchange process precludes a meaningful calculation of the exchange parameters using this technique) were determined from a series of $[^{31}P-^{31}P]$-EXSY spectra (e.g., Figure S9) recorded in the range of 238−253 K at different mixing times. Plots of the data are shown in Figure

https://dx.doi.org/10.1021/acs.inorgchem.0c02205
Inorg. Chem. XXXX, XXX, XXX−XXX

S10, and the kinetic Arrhenius plot is shown in Figure S11. The resultant activation energy, E_a, of 12.8 kcal mol^{-1} compares to the $\Delta G^{\ddagger}$ value of ca. 10.8 kcal mol^{-1} derived at the 238 K coalescence temperature.

Theoretical Calculations. Given the nonrigidity of the metal-to-borane linkage, we were interested in modeling the rotation of the ligand sphere in **2** using a DFT-calculated relaxed potential energy surface (PES) scan of the system. In this scan, we varied the dihedral angle defined by Ni(7)−C(27) and B(1)−B(5) with the numbering as shown in Figure 2. As the angle increases in 10° steps from the low-energy asymmetric conformation (Figure 5), and the metal group undergoes an anticlockwise rotation relative to the {η^4-$B_{10}H_{12}$} fragment, leading to a rise in energy as the isonitrile ligand approaches the midpoint between the asymmetric equatorial arrangement (the lowest-energy conformer) with the highest point about 6 kcal mol^{-1} above the minimum. It then falls toward the symmetric conformation and ends at a slightly higher energy, as expected. However, at the midpoint, a lower-energy conformation is indicated. This calculated intermediate exhibits a dangling dppe ligand that results from the dissociation of one Ni−P bond (Figure 5). The Ni(7)−P(1) distance, however, remains relatively constant and similar to that in the X-ray diffraction study.

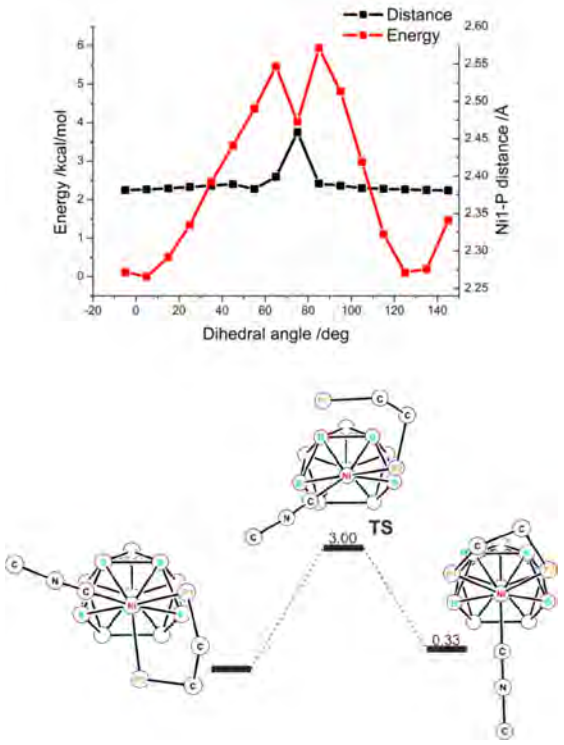

Figure 5. Graphs at the top represent the variations of energy and distance in the relaxed potential energy scan (PES) upon the rotation of the {dppe(EtNC)Ni} ligand sphere, using as a reference the dihedral angles defined by Ni(7)−C(27) and B(1)−B(5) (top graphs). The lower schematic illustrates the ligand orientations in the calculated species. (n.b. to reduce the computational load, methyl groups were used instead of ethyl groups on the isonitrile ligands).

We thus carried out a more accurate calculation of the transition state using the synchronous transit-guided quasi-Newton (STQN) method[30] implemented in *Gaussian 09* with the coordinates from the PES scan used as the initial coordinates in a QST3 calculation.[31] This resulted in a saddle point 3.0 kcal mol^{-1} above the minimum. This does not compare well to the measured value of the activation energy of the transition state, but this is not unexpected, as stated earlier, for this simple model with the organyl groups substituted by hydryls. In the transition state, the P(2) atom is now at a considerable distance of 3.82 Å from the nickel, and thus the {EtNC(L)Ni} moiety is tending toward regaining a 16-electron square-planar configuration and thereby opening itself up to further isonitrile ligand addition.

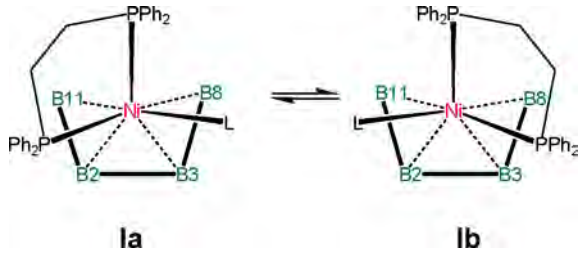

We carried out an additional geometry optimization on the transition state, releasing the constraint to reach the saddle point required in the STQN calculation, and this resulted in a stationary point 0.64 kcal mol^{-1} above the minimum at a Ni(7)−P(2) distance of 2.86 Å. This may approximately correspond to the midpoint lower-energy conformation initially indicated by the PES scan. The structural metrics to distinguish between the 18-electron and 16-electron configurations are not obvious in these two species. It may be noted, however, that the cluster B(9)−B(10) distances in **1** and **2** of

Scheme 4. Half-Rotational Metal-Flip Mechanism Similar to That Occurring in [8,8-$(PPh_3)_2$-*nido*-8,7-$RhSB_9H_{10}$][32]

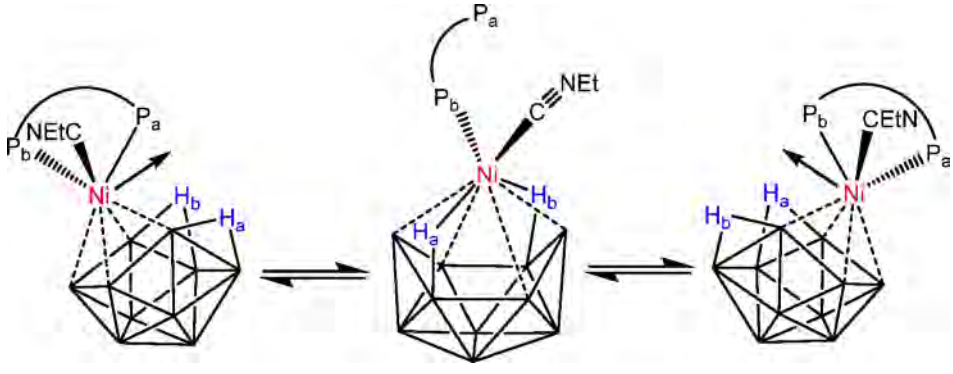

https://dx.doi.org/10.1021/acs.inorgchem.0c02205
Inorg. Chem. XXXX, XXX, XXX−XXX

1.990(5) and 1.918(7) Å, respectively, show a significant change due to the addition of the third CNEt ligand, and this change is paralleled in the calculated geometries of **1** and **2**, where these values are 1.999 and 1.933 Å, respectively. The calculated distance in the geometry-minimized transition state of 1.987 Å is therefore clearly closer to that in [(dppe)-$NiB_{10}H_{12}$] (**1**).

Thus, the fluxional process involving the exchange of all three proton resonances or all three phosphorus resonances is reasonably explained by the rotation of the metal−ligand sphere with respect to the cage, but we are unable to delineate the lower-energy, 10.8 kcal mol^{-1} rapid exchange process in the high-field AB system, which does not appear to involve the symmetric isomer. A 90° rocking (relative to the flat open face of the cluster) between the two enantiomers (schematic structures **Ia** and **Ib**) would render the phosphorus atoms equivalent. However, the calculation indicates that this is a higher-energy process by 6 kcal mol^{-1}. We are therefore currently unable to confidently delineate the lower-energy fluxional process. We investigated the possibility of a mechanism based on the half-rotational metal flip seen before in [8,8-$(PPh_3)_2$-*nido*-8,7-$RhSB_9H_{10}$][32] and represented in Scheme 4.

However, the activation energy for an intermediate with a 11-vertex pseudo-closo structure with a η^1-dppe ligand is also high.

Other rotamer intermediates may be present on the potential energy surface, but the small energy difference between this intermediate and the global minimum for the rotational process indicates that they will have a sufficiently long residence in solution compared to the transition state, facilitating reaction with the excess isonitrile. In this regard, compound **2** reacts with a large excess of CNEt to afford [$(EtNC)_3NiB_{10}H_{12}$] (**4**). This is illustrated in the ^{31}P NMR spectrum (Figure S12) in which the broader resonances characteristic of the {dppeNi} moiety have disappeared and only a sharp singlet due to free dppe is present. The boron spectrum (Table 1, Figure S13) remains essentially the same as in **2** with only small changes in chemical shifts. Removal of the isonitrile on a Schlenk line and redissolution in $CDCl_3$ returns **2**. The detailed proton spectrum for the *exo*-terminal hydrogen atoms in **4** was obscured by the intense isonitrile resonances although the bridging hydrogen atoms were observed at −2.14 ppm.

A possible mechanism for the substitution of the dppe ligand in **2** by isonitrile molecules would imply, therefore, the metal-to-borane rotational lability of the chelating ligand and subsequent coordination of one isonitrile to form a putative *bis*-EtNC-ligated cluster, [$(EtNC)_2(\eta^1$-dppe$)NiB_{10}H_{12}$]. Then, following the same reasoning, the rotation of the {$(EtNC)_2$(L)Ni} moiety would weaken the P−Ni bond, facilitating the complete substitution of the η^1-dppe ligand and leading to the formation of the tris-CNEt-ligated derivative (**4**) and free dppe.

Model for Ligand Substitution. To support this last hypothesis, we carried out a PES for the rotation of the {$(\eta^1$-dppe$)(EtNC)_2$Ni} ligand sphere with respect to the open face of the boron cluster (Figure 6). During the rotation, the remaining nickel phosphorus distance to the monodentate dppe ligand again increases from 1.83 Å to a nonbonding distance of 2.88 Å as it passes through the point approximately bisecting the B(2)−B(3) edge and parallel to the Ni(7)−B(1)−B(5) pseudo-mirror plane bisecting the molecule. When

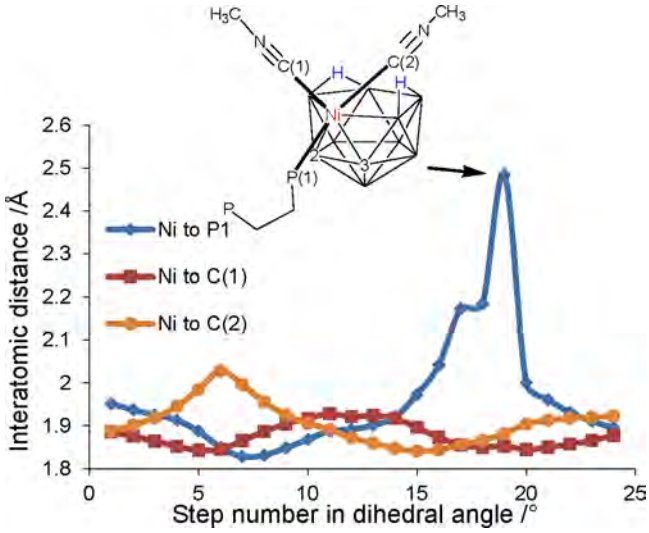

Figure 6. Relaxed potential energy scan (PES) of the rotation of the {(monodentate-dppe) $(MeNC)_2$Ni} ligand sphere with respect to the open face of the boron cluster. Distance Ni1 to P2 has 0.4 Å subtracted in order to normalize the plot.

the isonitrile passes through this position, the Ni(1)−C(1) distance lengthens from 1.86 to 2.03 Å. Clearly, the calculated 1.05 Å increase in the distance to P(1) is much greater than that for nickel-isonitrile and again opens the site for substitution in the presence of the excess isonitrile to form [$(EtNC)_3NiB_{10}H_{12}$] (**4**). Presumably, the chelating effect of the dppe ligand predominates in the reverse reaction, on removal of the excess isonitrile, to afford **2** again. It may be noted that the switch from bidentate to monodentate coordination for dppe has also been suggested from the DFT calculation of the reaction between [*nido*-(dppe)-$NiSB_9H_{11}$] and NH_3.[11] Similar to the reaction of **1** with isonitrile, NH_3 is shown to coordinate to the metal center in $CDCl_3$ solutions of [*nido*-(dppe)$NiSB_9H_{11}$] and to be removed on evaporation of the solution, quantitatively returning [*nido*-(dppe)$NiSB_9H_{11}$]. Therefore, the work herein tends to confirm the earlier hypothesis and to provide a mechanism for the NH_3 loss. It is notable that the rotational barrier is considerably lower in **2**, 12 kcal mol^{-1}, than in [$(PMe_2Ph)_2PtB_{10}H_{12}$], 19 kcal mol^{-1}, possibly suggesting that the metal ligand sphere is less strongly bonded to the cluster. In the isoelectronic and isostructural palladium analogue, [$(PMe_2Ph)_2PdB_{10}H_{12}$],[15] the value is 16 kcal mol^{-1}, indicating that the identity of the metal is one controlling factor. Other factors may be the steric effect of larger ligands and the increased number of ligands. Finally, it may be noted that the addition of the third ligand considerably lowers the barrier to rotation of the {dppe(L)Ni} moiety relative to that in **1**. A potential energy scan for **1** (Figure S14) returns a barrier of ca. 17 kcal mol^{-1} for the rotation of the {dppe(L)Ni} moiety.

In a final point, it may be noted that fluxional rotation of the metal−ligand sphere postulated for the monometallic compounds above may provide insight into the ability of dimetallic system [$L_4M_2B_{10}H_{10}$] described in the Introduction to reversibly take up small molecules across the metal−metal vector (Scheme 5). The dimetallic compound may be prepared by doubly deprotonating [$(PMe_2Ph)_2MB_{10}H_{12}$] and then adding a second metal as [$MCl_2(PMe_2Ph)_2$]. The long metal−metal distance (ca. 3 Å in the diplatinum compound)

https://dx.doi.org/10.1021/acs.inorgchem.0c02205
Inorg. Chem. XXXX, XXX, XXX−XXX

Scheme 5. (Upper) Reversible Uptake of Dioxygen on $[(PMe_2Ph)_4Pt_2B_{10}H_{10}]$ and (Lower) Illustration of the Proposed Fluxionality Observed in the NMR of Dioxygen Adduct $[(PMe_2Ph)_4(O_2)Pt_2B_{10}H_{10}]$

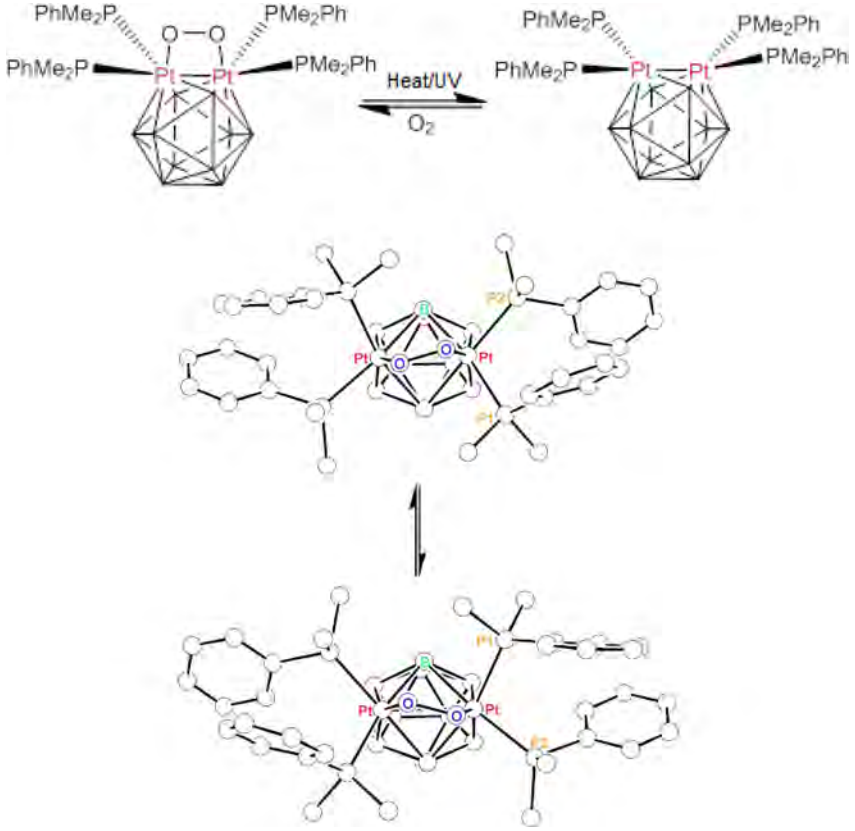

in the product is essentially nonbonding, and thus the two ends of the molecule can be regarded as resembling two 11-vertex *nido*-$\{(PMe_2Ph)_2Pt(II)B_{10}\}$ moieties[33] in which one oxygen occupies the third coordination position, similar to that in compounds **2** and **3**. On anaerobic dissolution in dichloromethane, dioxygen adduct $[(PMe_2Ph)_4(O_2)Pt_2B_{10}H_{10}]$ releases O_2 and forms an equilibrium mixture between the oxygenated and deoxygenated compounds. (SO_2 adduct $[(PMe_2Ph)_2Pt(SO_2)Pd(phenanthroline)B_{10}H_{10}]$ similarly forms equilibrium mixtures.[34]) Thus, it is reasonable to postulate that a rotation of the metal ligand spheres in this compound might be the initiating step in the expulsion of the dioxygen molecule. Indeed, variable-temperature NMR spectroscopy of $[(PMe_2Ph)_4(O_2)Pt_2B_{10}H_{10}]$ shows fluxional behavior that is interpreted as a flexing of the $\{O_2\}$ unit across the metal−metal vector and an interconversion between the mirror images of the molecules as shown in Scheme 5.[35] The activation energy of the process was $\Delta G^{\ddagger} = 9.0$ kcal mol^{-1}. A rotation, or a rocking, of the $\{(PMe_2Ph)_2Pt\}$ moiety could account for this observation, and a rough PES scan on one end of the molecule (clearly the process would occur simultaneously on both sides of the molecule) at the B3LYP/6-31G* LANL2DZ level in the manner of the above calculation for the nickelaboranes shows the Pt−O distance increasing from 2.2 to 2.4 Å (Figure S15), a result that is therefore indicative of a weakening of the binding of the oxygen to the metal center.

CONCLUSIONS

This article describes the synthesis and structural characterization of [7,7-(dppe)-*nido*-7-$NiB_{10}H_{12}$] (**1**) and its small-molecule EtNC and CO adducts, [(EtNC)(dppe)-*nido*-$NiB_{10}H_{12}$] (**2**) and [(CO)(dppe)-*nido*-$NiB_{10}H_{12}$] (**3**), and delineates the dynamic molecular behavior of all of these species in solution. Thus, compounds [(EtNC)(dppe)-*nido*-$NiB_{10}H_{12}$] (**2**) and [(CO)(dppe)-*nido*-$NiB_{10}H_{12}$] (**3**), in their variable-temperature ^{31}P and ^{1}H NMR behavior, exhibit a fluxional contra-rotation of the ligand sphere with respect to the borane cage. DFT modeling in the case of **2** indicates that, during the rotation, a Ni−P bond weakens sufficiently for one end of the dppe ligand to detach from the metal, resulting in a square-planar nickel center with a vacant coordination site which may then, in solution and in the presence of excess isonitrile, take up another EtNC ligand. Computational modeling of this system then suggests that a further rotation of the resultant $\{(monodentate\text{-}dppe)(EtNC)_2Ni\}$ moiety causes a similar weakening of the remaining Ni−P linkage, allowing for a third isonitrile to enter the ligand sphere and attach to the nickel center, completely displacing the dppe. This model is observed experimentally in the NMR study of the formation of $[(EtNC)_3NiB_{10}H_{12}]$ (**4**) from solutions of **2** in excess EtNC. Subsequent removal of the excess isonitrile regenerates compound **2**, thereby revealing the reversibility of this behavior. This type of metal-to-borane rotation, found previously in another metallaborane system, $[(PMe_2Ph)_2PtB_{10}H_{12}]$,[14] has until now been no more than an academic curiosity with its only practical manifestation being in the NMR properties of participating compounds. In our current work, however, we progress to describe the chemical consequences of such an intramolecular dynamic, showing it to cause the expulsion of metal ligands and consequently open a coordination vacancy on the metal center of the molecule. This revelation has, in turn, led us to

https://dx.doi.org/10.1021/acs.inorgchem.0c02205
Inorg. Chem. XXXX, XXX, XXX−XXX

reconsider the mechanism of the reversible release of sequestered small molecules such as CO and O_2 in the previously reported bimetalladodecaboranyl compounds, $[L_4(CO)M_2B_{10}H_{10}]$ and $[L_4(O_2)M_2B_{10}H_{10}]$.[6,35] The current results may suggest that it is the rotation of phosphine ligands on the $[L_4M_2B_{10}H_{10}]$ system that may trigger the release of CO or O_2. In every case, this information sets a foundation from which more advanced work on this and other metallaborane systems can be conceived and provides a more general reference of how NMR spectroscopy can be used to analyze the precise locomotion of labile ligands around a metal center held within a borane cluster.

EXPERIMENTAL SECTION

Reactions were carried out under an argon atmosphere using standard Schlenk line techniques. Dry oxygen-free solvents were obtained using an Innovative Technology Inc. solvent purification system. $[NiCl_2(dppe)]$ and $Li[BHEt_3]$, 1 M solutions in tetrahydrofuran, were purchased from Acros and used as received. Preparative thin-layer chromatography (TLC) was carried out using 1 mm layers of silica gel G (Macherey-Nagel silica gel G/UV254) made from water slurries on glass plates with dimensions of 20 × 20 cm^2 and dried in air at 80 °C. Infrared spectra were recorded on a PerkinElmer Spectrum 100 spectrometer using a Universal ATR sampling accessory. NMR spectra were recorded on JEOL 600 MHz, Bruker Avance 300 MHz, and AV 400 and 500 MHz spectrometers using ^{11}B, $^{11}B-\{^1H\}$ ^1H, $^1H-\{^{11}B\}$, and $^1H-\{^{11}B(selective)\}$ and 2D EXSY[28] techniques. ^1H NMR chemical shifts were measured relative to partially deuterated solvent peaks but are reported in ppm relative to tetramethylsilane. ^{11}B chemical shifts are quoted relative to $[F_3B(OEt_2)]$, and ^{31}P chemical shifts are quoted relative to 85% aqueous H_3PO_4. Mass spectrometric data were recorded on a MICROFLEX instrument operating in either positive or negative mode, using matrix-assisted laser desorption/ionization (MALDI). A 337 nm nitrogen laser (photon energy of 3.68 eV) was used for the ionization process, and the molecules under study were protected with a matrix of *trans*-2-[3-(4-*tert*-butylphenyl)-2-methyl-2-propenylidene] malononitrile (DCTB).

[(dppe)NiB$_{10}$H$_{12}$] (1). $K[BHEt_3]$ (2.06 mL, 2.06 mmol in THF) was slowly injected into a stirred solution of $B_{10}H_{14}$ (0.126g, 1.03 mmol) in 70 mL of diethyl ether. A pale-yellow solution containing a pale-yellow solid was formed. Against a flow of argon, $[NiCl_2(dppe)]$ (0.544 g, 1.03 mmol) was added and the mixture was left to stir overnight. The next day, the reaction mixture was filtered through a column of silica gel and washed through with toluene and then CH_2Cl_2. An orange band moved down the column, and the resultant CH_2Cl_2 solution was reduced in volume and cyclohexane was added, giving a dark-orange precipitate. The solid showed a single product by ^{11}B NMR, which was identified as [7,7-(dppe)-*nido*-7-$NiB_{10}H_{12}$] (0.201 g, 0.347 mmol, 34%). Anal. meas (calcd) for $C_{27}H_{37}B_{10}Cl_3NiP_2$: C, 46.13 (46.54); H, 5.61 (5.35). Single crystals suitable for X-ray diffraction analysis were obtained from $CHCl_3$/*n*-hexane solution. We were unable to obtain mass spectrometry data for this compound using the techniques available to us, although, as seen below, the isonitrile adduct did give an isotope envelope attributable to $[(dppe)NiB_{10}H_{12}]$ (**1**). NMR data are listed in Tables 1 and 2.

[(EtNC)(dppe)NiB$_{10}$H$_{12}$] (2). $[(dppe)NiB_{10}H_{12}]$ (10.5 mg, 13.3 μmol) was weighed into a Schlenk tube containing a stir bar, which was then evacuated and refilled with argon. Dichloromethane (ca. 10 mL) was injected through a septum. The solution was frozen in liquid nitrogen and evacuated. EtNC was then condensed in the vessel, and the tube was sealed (tap). After stirring at room temperature for 1 h, a clear red-orange solution was obtained. A test TLC (silica foil) showed one orange spot. Preparative TLC gave one orange band on the plate (R_f = 0.5, 100% CH_2Cl_2). The band was removed and washed off of the silica gel with CH_2Cl_2. The solvent was removed by evaporation, and the resultant solid was 11.2 mg (13.3 μmol, 100%) of $[EtNC(dppe)NiB_{10}H_{12}]$. IR: νNC, 2202; νBH, 2520, 2500, 2479sh. Anal. meas (calcd): C, 53.84 (55.08); N, 2.1 (2.21); H, 6.53 (6.36). NMR data are listed in Tables 1, 2, and S1. The IR stretching frequency of the coordinated isonitrile is 2202 cm^{-1}, which is compared to that of the free uncoordinated molecule[36] at 2151 cm^{-1}. Single crystals were obtained by hexane diffusion into a dichloromethane solution of the compound. Mass spectrometry showed an isotope envelope centered at 577, matching the calculated pattern for [M−EtNC], $C_{26}H_{36}P_2NiB_{10}$. In a separate experiment, $CDCl_3$ (ca. 0.5 mL) was condensed onto $[(dppe)NiB_{10}H_{12}]$ (11.2 mg, 19.4 μmol) in a Young's NMR tube, and ca. 1 equiv of EtNC was condensed into the tube. ^{11}B NMR spectroscopy showed mainly product **2** plus a number of minor peaks. A red solid, later identified as compound **2**, precipitated from solution and floated to the top of the liquid. After the addition of another 1 equiv of EtNC, all of the minor peaks had disappeared and a weak ^{11}B spectrum of **2** was obtained. The compound is only moderately soluble in $CDCl_3$ (or CD_3CN), and NMR characterization was carried out in CD_2Cl_2 solution. NMR data are listed in Tables 1, 2, and S1.

[(CO)(dppe)NiB$_{10}$H$_{12}$] (3). An unmeasured quantity of CO gas was condensed into a high-pressure NMR tube under liquid nitrogen containing a CD_2Cl_2 solution of $[(dppe)NiB_{10}H_{12}]$ (**1**). The tube was sealed and allowed to warm to ambient temperature, during which time a red band formed at the top of the orange solution, which slowly suffused down the tube. Multielement NMR spectra of the resultant red solution were measured (Tables 1 and 2). The facile loss of CO when the compound was removed from the CO atmosphere precluded the measurement of the infrared CO stretching frequency.

X-ray Diffraction. Intensities were collected using a Bruker SMART APEX-DUO diffractometer with graphite-monochromated Mo Kα radiation (λ = 0.71073 Å) following standard procedures. Intensities were integrated and corrected for absorption effects using the SAINT+ and SADABS programs, included in the APEX2 package.[37,38] The structure was solved by the Patterson method. All non-hydrogen atoms were located in the subsequent Fourier maps. Refinement was carried out by a full-matrix least-squares procedure (based on F_0^2) using anisotropic temperature factors for all non-hydrogen atoms. Most C−H hydrogen atoms were placed in calculated positions with fixed isotropic thermal parameters (1.2 × U_{equiv} of the parent carbon atom).

Crystal data for compound **1**, CCDC 1569292: M = $C_{27}H_{37}B_{10}Cl_3NiP_2$, orange prism, 0.180 × 0.140 × 0.070 mm^3, monoclinic, space group $P21/n$, V = 3347.6(4) $Å^3$, Z = 4, D_c = 1.382 g/cm^3, F_{000} = 1432, T = 100(2) K, $2\theta_{max}$ = 52.7°, 34 775 reflections collected, 6840 unique (R_{int} = 0.0561). Final GoF = 1.015, $R1$ = 0.0399, $wR2$ = 0.0808, R indices based on 5109 reflections with $I > 2\sigma(I)$ (refinement on F^2), 436 parameters, 0 restraints. Lp and absorption corrections applied, μ = 0.935 mm^{-1}.

Crystal data for compound **2**, CCDC 1569293: M = $C_{29}H_{41}B_{10}NNiP_2$, red prism, 0.260 × 0.070 × 0.060 mm^3, monoclinic, space group $P21/n$, V = 3209.3(5) $Å^3$, Z = 4, D_c = 1.309 g/cm^3, F_{000} = 1320 T = 100(2) K, $2\theta_{max}$ = 50.1°, 29 247 reflections collected, 5648 unique (R_{int} = 0.0839). Final GoF = 1.195, $R1$ = 0.0636, $wR2$ = 0.0958, R indices based on 4127 reflections with $I > 2\sigma(I)$ (refinement on F^2), 437 parameters, 0 restraints. Lp and absorption corrections applied, μ = 0.727 mm^{-1}.

See also Table S2.

DFT Calculations. Calculations were performed using the *Gaussian 09* package.[31] Structures were modeled using hydrogen atoms rather than organyl groups on the dppe ligands in order to reduce the computation time. The structures were initially optimized using standard methods with the STO-3G* basis set for B, P, and H. The final optimizations, including frequency analyses to confirm the true minima, together with GIAO NMR nuclear-shielding predictions, were performed at the B3LYP/6-31+G(d,p) level. Calculated ^{11}B shielding values were related to chemical shifts by comparison with the computed value for B_2H_6 which was taken to be $\delta(^{11}B)$ + 16.6 ppm relative to the $[F_3B(OEt_2)]$ = 0.0 ppm standard.

https://dx.doi.org/10.1021/acs.inorgchem.0c02205
Inorg. Chem. XXXX, XXX, XXX−XXX

■ ASSOCIATED CONTENT

Supporting Information

The Supporting Information is available free of charge at https://pubs.acs.org/doi/10.1021/acs.inorgchem.0c02205.

NMR spectra for compounds **1**−**4** including EXSY and variable-temperature spectra; kinetic and Arrhenius plots for **2**; DFT-calculated Cartesian atomic coordinates for compounds **2** and **3** and relaxed potential energy scan plots; calculations of the free energy of activation by the coalescence temperature for **2**; and crystal data and structure refinement details for **1** and **2** (PDF)

Accession Codes

CCDC 1569292−1569293 contain the supplementary crystallographic data for this paper. These data can be obtained free of charge via www.ccdc.cam.ac.uk/data_request/cif, or by emailing data_request@ccdc.cam.ac.uk, or by contacting The Cambridge Crystallographic Data Centre, 12 Union Road, Cambridge CB2 1EZ, UK; fax: +44 1223 336033.

■ AUTHOR INFORMATION

Corresponding Authors

Jonathan Bould − *Institute of Inorganic Chemistry, Academy of Sciences of the Czech Republic, Husinec-Řež 250 68, Czech Republic; Instituto de Síntesis Química y Catálisis Homogénea-ISQCH, University of Zaragoza 12, 50009 Zaragoza, Spain;* orcid.org/0000-0003-3615-1938; Email: jbould@gmail.com

Ramón Macías − *Instituto de Síntesis Química y Catálisis Homogénea-ISQCH, University of Zaragoza 12, 50009 Zaragoza, Spain;* orcid.org/0000-0003-2299-9428; Email: rmacias@unizar.es

Authors

Oleg Tok − *Institute of Inorganic Chemistry, Academy of Sciences of the Czech Republic, Husinec-Řež 250 68, Czech Republic*

Vincenzo Passarelli − *Instituto de Síntesis Química y Catálisis Homogénea-ISQCH, University of Zaragoza 12, 50009 Zaragoza, Spain;* orcid.org/0000-0002-1735-6439

Michael G. S. Londesborough − *Institute of Inorganic Chemistry, Academy of Sciences of the Czech Republic, Husinec-Řež 250 68, Czech Republic;* orcid.org/0000-0002-6161-6592

Complete contact information is available at: https://pubs.acs.org/10.1021/acs.inorgchem.0c02205

Notes

The authors declare no competing financial interest.

■ ACKNOWLEDGMENTS

The authors gratefully acknowledge the support of the Spanish Ministerio de Ciencia, Innovación y Universidades under reference no. PGC2018-099383-B-I00. We acknowledge the use of Servicio General de Apoyo a la Investigación-SAI, Universidad de Zaragoza. J.B. and M.G.S.L. also acknowledge support from the Czech Science Foundation and project no. 18-20286S.

■ REFERENCES

(1) Wesemann, L. *s*- and *p*-Block Heteroboranes and Carboranes. *Comprehensive Organometallic Chemistry III* **2007**, 113−131.

(2) Kennedy, J. D. The Polyhedral Metallaboranes Part II. Metallaborane Clusters with Eight Vertices and More. *Prog. Inorg. Chem.* **2007**, 211−434.

(3) Kennedy, J. D. The Polyhedral Metallaboranes Part I. Metallaborane Clusters with Seven Vertices and Fewer. *Prog. Inorg. Chem.* **2007**, 519−679.

(4) Alvarez, A.; Macías, R.; Bould, J.; Fabra, M. J.; Lahoz, F. J.; Oro, L. A. Alkene hydrogenation on an 11-vertex rhodathiaborane with full cluster participation. *J. Am. Chem. Soc.* **2008**, *130* (34), 11455−11466.

(5) Macías, R. Reactions of Unsaturated Organic Molecules and H_2 on Metallaboranes and Metallathiaboranes with Full Metal−Borane−Ligand Cooperation. *Handbook of Boron Science* **2018**, *2*, 81−116.

(6) Bould, J.; Baše, T.; Londesborough, M. G. S.; Oro, L. A.; Macías, R.; Kennedy, J. D.; Kubát, P.; Fuciman, M.; Polívka, T.; Lang, K. Reversible Capture of Small Molecules On Bimetallaborane Clusters: Synthesis, Structural Characterization, and Photophysical Aspects. *Inorg. Chem.* **2011**, *50* (16), 7511−7523.

(7) Bould, J.; Londesborough, M. G. S.; Kennedy, J. D.; Macías, R.; Winter, R. E. K.; Císařová, I.; Kubat, P.; Lang, K. Isonitrile ligand effects on small-molecule-sequestering in bimetalladodecaborane clusters. *J. Organomet. Chem.* **2013**, *747*, 76−84.

(8) Álvarez, A.; Macías, R.; Bould, J.; Cunchillos, C.; Lahoz, F. J.; Oro, L. A. Alkyne-Promoted H_2 Loss in a Metallaborane: *Nido*-to-*Closo* Cluster Transformation and sp C-H Bond Oxidative Addition. *Chem. - Eur. J.* **2009**, *15* (22), 5428−5431.

(9) Álvarez, A.; Macías, R.; Fabra, M. J.; Lahoz, F. J.; Oro, L. A. Reversible Ethylene Dihydrogen Mediated 11-Vertex *nido* → *closo* → *nido* Conversion in a Metallathiaborane Cluster. *J. Am. Chem. Soc.* **2008**, *130* (7), 2148−2149.

(10) Calvo, B.; Macías, R.; Artigas, M. J.; Lahoz, F. J.; Oro, L. A. Proton-Assisted Hydrogen Activation on Polyhedral Cations. *Chem. - Eur. J.* **2013**, *19* (12), 3905−3912.

(11) Bould, J.; Passarelli, V.; Oro, L. A.; Macías, R. Reversible Small-Molecule Interactions with Coordinatively Unsaturated Metal Centers Held in Metallathiaborane Clusters. *Eur. J. Inorg. Chem.* **2017** (38−39), 4599−4617.

(12) Macías, R.; Rath, N. P.; Barton, L. Organometallic Chemistry on a Metallathiaborane Cluster: Reactions of [8,8-$(PPh_3)_2$-*nido*-8,7-$RhSB_9H_{10}$] with Bidentate Phosphine Ligands. *Organometallics* **1999**, *18* (18), 3637−3648.

(13) Beckett, M. A.; Greenwood, N. N.; Kennedy, J. D.; Thornton-Pett, M. Preparation, crystal and molecular structure of, and NMR parameters for, the exopolyhedral heterocyclic platinaundecaborane [μ-2,7-(SCSNEt$_2$)-7-(PMe_2Ph)-*nido*-7-$PtB_{10}H_{11}$]. *Polyhedron* **1985**, *4* (3), 505−511.

(14) Boocock, S. K.; Greenwood, N. N.; Kennedy, J. D.; McDonald, W. S.; Staves, J. The chemistry of isomers of icosaborane(26), $B_{20}H_{26}$: synthesis and nuclear magnetic resonance study of various isomers of platinahenicosaboranes and diplatinadocosaboranes, and the X-ray crystal and molecular structures of 7,7-bis(dimethylphenylphosphine)-*nido*-7-platinaundecaborane and 4-(2′-*nido*-decaboranyl)-7,7-bis(dimethylphenylphosphine)-*nido*-7-platinaundecaborane. *J. Chem. Soc., Dalton Trans.* **1981**, *12*, 2573−2584.

(15) Londesborough, M. G. S.; O'Dowd, C.; Bould, J.; Barrett, S. A.; Kilner, C. A.; Thornton-Pett, M.; Kennedy, J. D. Polyhedral palladaborane chemistry: isolation and structural characterization of ten-vertex $(PMe_2Ph)_2PdB_9H_{12}(PMe_2Ph)$ and eleven-vertex $(PMe_2Ph)_2PdB_{10}H_{12}$. *J. Chem. Crystallogr.* **2000**, *30* (5), 283−289.

(16) Cordero, B.; Gómez, V.; Platero-Prats, A. E.; Revés, M.; Echeverría, J.; Cremades, E.; Barragán, F.; Alvarez, S. Covalent radii revisited. *Dalton Trans.* **2008**, *21*, 2832−2838.

(17) Wade, K. Structural and Bonding Patterns in Cluster Chemistry. *Adv. Inorg. Chem. Radiochem.* **1976**, *18*, 1−66.

(18) Wade, K. The structural significance of the number of skeletal bonding electron-pairs in carboranes, the higher boranes and borane anions, and various transition-metal carbonyl cluster compounds. *J. Chem. Soc. D* **1971**, *15*, 792−793.

(19) Williams, R. E. Coordination number pattern recognition theory of carborane structures. *Adv. Inorg. Chem. Radiochem.* **1976**, *18*, 67−142.
(20) Kennedy, J. D. In *The Borane-Carborane-Carbocation Continuum*; Casanova, J., Ed.; Wiley: New York, 1998; Chapter 3, pp 85−116.
(21) Bould, J.; Macías, R. Do agostic interactions play a role in the stabilization of the nido structure of $[(PPh_3)_2RhSB_9H_{10}]$? *J. Organomet. Chem.* **2014**, *761*, 120−122.
(22) Bould, J.; Teat, S. J.; Kennedy, J. D. Polyhedral dipalladaborane chemistry. The molecular structure and cluster electron count of 7,8-$(PPh_3)_2$-7,8-(μ-PPh_2)-9,11-$(OEt)_2$-*nido*-7,8-$Pd_2B_9H_8$. *Collect. Czech. Chem. Commun.* **2007**, *72* (12), 1631−1638.
(23) Adams, K. J.; McGrath, T. D.; Rosair, G. M.; Weller, A. S.; Welch, A. J. Rhodathiaboranes with 'anomalous' electron counts: synthesis, structure and reactivity. *J. Organomet. Chem.* **1998**, *550* (1), 315−329.
(24) Wolinski, K.; Hinton, J. F.; Pulay, P. Efficient implementation of the gauge-independent atomic orbital method for NMR chemical shift calculations. *J. Am. Chem. Soc.* **1990**, *112* (23), 8251−8260.
(25) Kennedy, J. D.; Wrackmeyer, B. An NMR investigation of the $[B_{10}H_{12}]^{2-}$ ligand in $[Pt(B_{10}H_{12})(PMe_2Ph)_2]$. *J. Magn. Reson. (1969-1992)* **1980**, *38* (3), 529−535.
(26) Cotton, F. A. Fluxional organometallic molecules. *Acc. Chem. Res.* **1968**, *1* (9), 257−265.
(27) Shanan-Atidi, H.; Bar-Eli, K. H. A convenient method for obtaining free energies of activation by the coalescence temperature of an unequal doublet. *J. Phys. Chem.* **1970**, *74* (4), 961−963.
(28) Perrin, C. L.; Dwyer, T. J. Application of two-dimensional NMR to kinetics of chemical exchange. *Chem. Rev.* **1990**, *90* (6), 935−967.
(29) Farrugia, L. J. Dynamics and fluxionality in metal carbonyl clusters: some old and new problems. *J. Chem. Soc., Dalton Trans.* **1997**, *11*, 1783−1792.
(30) Peng, C.; Bernhard Schlegel, H. Combining Synchronous Transit and Quasi-Newton Methods to Find Transition States. *Isr. J. Chem.* **1993**, *33* (4), 449−454.
(31) Frisch, M. J.; Trucks, G. W.; Schlegel, H. B.; Scuseria, G. E.; Robb, M. A.; Cheeseman, J. R.; Scalmani, G.; Barone, V.; Mennucci, B.; Petersson, G. A.; Nakatsuji, H.; Caricato, M.; Li, X.; Hratchian, H. P.; Izmaylov, A. F.; Bloino, J.; Zheng, G.; Sonnenberg, J. L.; Hada, M.; Ehara, M.; Toyota, K.; Fukuda, R.; Hasegawa, J.; Ishida, M.; Nakajima, T.; Honda, Y.; Kitao, O.; Nakai, H.; Vreven, T.; Montgomery, J. A.; Peralta, J. E.; Ogliaro, F.; Bearpark, M.; Heyd, J. J.; Brothers, E.; Kudin, K. N.; Staroverov, V. N.; Keith, T.; Kobayashi, R.; Normand, J.; Raghavachari, K.; Rendell, A.; Burant, J. C.; Iyengar, S. S.; Tomasi, J.; Cossi, M.; Rega, N.; Millam, J. M.; Klene, M.; Knox, J. E.; Cross, J. B.; Bakken, V.; Adamo, C.; Jaramillo, J.; Gomperts, R.; Stratmann, R. E.; Yazyev, O.; Austin, A. J.; Cammi, R.; Pomelli, C.; Ochterski, J. W.; Martin, R. L.; Morokuma, K.; Zakrzewski, V. G.; Voth, G. A.; Salvador, P.; Dannenberg, J. J.; Dapprich, S.; Daniels, A. D.; Farkas, O.; Foresman, J. B.; Ortiz, J. V.; Cioslowski, J.; Fox, D. J. *Gaussian 09*, Revision D.01; Gaussian Inc.: Wallingford, CT, 2013.
(32) Macías, R.; Bould, J.; Holub, J.; Kennedy, J. D.; Štíbr, B.; Thornton-Pett, M. Polyhedral metallaheteroborane chemistry. Synthesis, spectroscopy, structure and dynamics of eleven-vertex {RhNB9} and {PtCB9} metallaheteroboranes. *Dalton Trans.* **2007**, *27*, 2885−2897.
(33) Bould, J.; Císařová, I.; Kennedy, J. D. Polyhedral Platinaborane Chemistry. Interaction of PMe_2Ph with $[(PMe_2Ph)_2PtB_{10}H_{12}]$. *Organometallics* **2012**, *31* (7), 2691−2696.
(34) Bould, J.; Kennedy, J. D. Metallaborane reaction chemistry. A predicted and found tailored facile and reversible capture of SO_2 by a B-frame-supported bimetallic: structures of $(PMe_2Ph)_2PtPd(phen)$-$B_{10}H_{10}$ and $(PMe_2Ph)_2Pt(SO_2)Pd(phen)B_{10}H_{10}$. *Chem. Commun.* **2008**, *21*, 2447−2449.
(35) Bould, J.; Kilner, C. A.; Kennedy, J. D. The capture of dioxygen, carbon monoxide and sulfur dioxide by $(PMe_2Ph)_4Pt_2B_{10}H_{10}$. *Dalton Trans.* **2005**, *9*, 1574−1582.
(36) Stephany, R. W.; de Bie, M. J. A.; Drenth, W. A ^{13}C-NMR and IR study of isocyanides and some of their complexes. *Org. Magn. Reson.* **1974**, *6* (1), 45−47.
(37) *SAINT+*, version 6.01; Bruker AXS, Inc.: Madison, WI, 2001.
(38) Sheldrick, G. M. *SABADS*; University of Göttingen: Göttingen, Germany, 1999.

https://dx.doi.org/10.1021/acs.inorgchem.0c02205
Inorg. Chem. XXXX, XXX, XXX−XXX